Electrochimica Acta 286 (2018) 339–349

Contents lists available at ScienceDirect

Electrochimica Acta

journal homepage: www.elsevier.com/locate/electacta

# Corrosion investigation of the 18Ni 300 grade maraging steel in aqueous chloride medium containing $H_2S$ and $CO_2$

Archimedes F. Avelino [a], Walney S. Araújo [a], Diego F. Dias [b], Luis Paulo M. dos Santos [c], Adriana N. Correia [c], Pedro de Lima-Neto [c, *]

[a] Departamento de Engenharia Metalúrgica e Materiais, Universidade Federal do Ceará, Campus do Pici, bloco 729, 60440-900 Fortaleza, CE, Brazil
[b] Programa de Pós-Graduação em Física, Universidade Federal do Ceará, Campus do Pici, bloco 922, 60440-900 Fortaleza, CE, Brazil
[c] Departamento de Química Analítica e Físico-Química, Universidade Federal do Ceará, Campus do Pici, bloco 940, 60440-900 Fortaleza, CE, Brazil

ARTICLE INFO

*Article history:*
Received 22 March 2018
Received in revised form
18 July 2018
Accepted 9 August 2018
Available online 10 August 2018

*Keywords:*
Maraging steel
Electrochemical techniques
$H_2S$ corrosion
$CO_2$ corrosion
Austenitic phase
Aging thermal treatment

ABSTRACT

The corrosion behavior of the 18Ni 300-grade maraging steel in 0.6 mol $L^{-1}$ NaCl solution, containing 1 mmol $L^{-1}$ $H_2S$, and saturated with $CO_2$, was investigated by measurement of the open circuit potential, potentiodynamic polarization and electrochemical impedance spectroscopy techniques. The maraging steel was solution-treated at 840 °C for 1 h and aged at 650 °C for 3 h. All corrosion electrochemical tests proved that the austenitic phase formed during the aging thermal treatment was detrimental to corrosion resistance of the 18Ni 300-grade maraging steel. The analysis of the XPS spectra suggested that $FeCO_3$, $Fe_2O_3$, $FeS_2$, $FeSO_4$, NiO, $Ni(OH)_2$, NiS, $NiSO_4$, $MoO_2$, $MoO_3$ and $MoS_2$ were the corrosion products deposited on the surface of both maraging steel samples after 29 days of immersion in the testing solution. Lastly, for industrial application requiring the corrosion resistance property of the 18Ni 300 grade maraging steel, it is recommended that it be thermal solution-treated before its use.



## 1. Introduction

It is well known that maraging steels gain hardness after aging thermal treatment between 400 and 650 °C [1]. Some authors reported that the phases formed between 400 and 480 °C, $Ni_3Ti$ and $Ni_3Mo$, are responsible for the hardness gained during the initial stages of thermal treatment [2–4]. On the other hand, aging procedures at higher temperatures, e.g. 650 °C for 3 h, promotes the dissolution of both phases and the formation of $Fe_2Mo$ stable precipitates and a Ni enrichment of the matrix, which causes the formation of the austenite phase [5–7]. Due to their mechanical resistance associated to the annealing process, maraging steels are used in pressure vessels, aircraft components, missile and rocket motor cases, nuclear and gas turbine applications [8].

In the current decade, it is increasing the interest on corrosion resistance properties of these alloys. For instance, it was showed that thermal aged maraging specimens were more susceptible to corrosion than the thermal solution-treated specimens in slightly acid radioactive water [9], in phosphoric acid and in sulfuric acid media [10,11] and that $Ce^{3+}$ ions and some organic molecules inhibited the corrosion of maraging steels in acid solutions [12–17]. In addition, Santos et al. [18] showed that the specimens of 18% Ni 300-grade maraging steel aged at 480 °C and at 570 °C, for a period of 3 h, were more susceptible to hydrogen embrittlement than solution annealed ones, Manwatkar et al. [19] investigated the stress corrosion resistance of a maraging steel 250-grade shear bolt used in the interstage structure of a satellite launch vehicle and showed that the crack initiated from pits, Seikh et al. [20] produced a cobalt-free maraging steel by electroslag remelting (ESR) technique and demonstrated that the produced maraging steel was more corrosion resistant than the commercial C250 maraging steel in 1 mol $L^{-1}$ $H_2SO_4$ solution, Tian et al. [21] produced a new maraging stainless steel to evaluate the synergistic effect between Co and Cr and showed that the produced alloy presented higher corrosion resistance in 3.5% NaCl solution than the 15-4PH stainless steel and, finally, Meshram et al. [22] used the friction stir welding process for welding the 18%Ni 250-grade maraging steel and they showed that the welded joints presented fine grain structure, absence of segregation of alloying elements and higher resistance to stress corrosion crack compared to base metal and gas tungsten arc weldments.

* Corresponding author.
*E-mail address:* pln@ufc.br (P. de Lima-Neto).

https://doi.org/10.1016/j.electacta.2018.08.042
0013-4686/

In oilfield production, oilfield formation water is co-extracted with the oil and it contains chloride ions and can also contain $CO_2$ (sweet corrosion) and $H_2S$ (sour corrosion) dissolved in the produced fluids, which represents a significant problem for the oil and gas industry since 1940 [23]. The mild steel is usually the most cost-effective for oil and gas facilities, but its corrosion resistance is strongly affected by the presence of these chemical species in the aqueous medium. The maraging steels can be a potential alternative to the carbon steel, since these alloys have better corrosion resistance than the carbon steel. However, the corrosion behavior of the maraging steel in aqueous media containing $CO_2$ and $H_2S$ is unknown. For carbon steel, results have shown that $H_2S$ exhibited an acceleration of the anodic reactions (carbon steel dissolution). However, under certain special conditions, such as $H_2S$ concentration less than 0.04 mmol $L^{-1}$ and with pH value varying between 3 and 5, the $H_2S$ causes an inhibition of the steel corrosion [24–27]. The occurrence of this inhibition effect was related to the deposition of the ferrous sulfide on steel surface, which acts as a protective layer. The formation of the protective barrier is related to the $H_2S$ concentration in the electrolyte, to the pH of the solution and to the immersion time of steel in the corrosive medium [28–31]. The chemical composition of the protective film revealed the presence of several ferrous sulfide, such as pyrite ($FeS_2$, cubic), troilite (FeS), pyrrhotite ($FeS_{1-x}$) and mackinawite ($Fe_3S_4$) [32,33].

Dissolved in brine aqueous solution, $CO_2$ is deleterious to the corrosion resistance of the metallic materials, since the dissolved $CO_2$ reacts with water to form the carbonic acid, leading to the decrease of the pH about 4 [34–41]. Investigations have identified that iron carbonate ($FeCO_3$) was the main corrosion product deposited on steel surface [40–42].

In presence of $CO_2$ and $H_2S$, both iron carbonate and iron sulphide scales can be formed on the steel surface, acting as a barrier that causes the reduction of the corrosive process and preventing the underlying steel from further dissolution. Studies on the effect of very small $H_2S$ concentrations on $CO_2$ corrosion at low pH have been reported [24,27,43–46] and the data strongly suggested that the presence of very small amounts of $H_2S$ leads to a significant reduction of the iron corrosion in $CO_2$ environments [47].

Thus, the aim of this investigation was to study the influence of the aging thermal treatment at 650 °C for 3 h on the corrosion resistance of 18Ni 300-grade maraging steel in 0.6 mol $L^{-1}$ NaCl solution, saturated with $CO_2$ and containing 1 mmol $L^{-1}$ $H_2S$. This investigation will be beneficial to understand the feasibility of this steel be applied in oil industry.

## 2. Experimental details

### 2.1. Sample preparation

A 18Ni 300 grade maraging steel was used as working electrode, and its chemical composition is displayed in Table 1. The steel samples had the dimensions of 10 mm × 10 mm × 8 mm and were solution-treated at 840 °C for 1 h, rapidly cooled in water and followed by an aging treatment at 650 °C for 3 h and subsequently quenched in water.

For electrochemical corrosion tests, the 18Ni 300 grade maraging steel samples were embedded in epoxy resin, leaving exposed a quadrangular geometric surface area (*circa* 0.1 $cm^2$). Prior to each electrochemical experiment, the coupons were sanded with 100, 220, 360, 400 and 600 SiC emery papers, washed with distilled water, degreased in acetone and dried with heated air flow.

**Table 1**
Composition of the 18Ni 300 grade maraging steel.

| Element | Fe | Ni | Co | Mo | Ti | Al | C |
|---|---|---|---|---|---|---|---|
| w % | Balance | 18.7 | 9.62 | 4.84 | 0.87 | 0.39 | <0.03 |

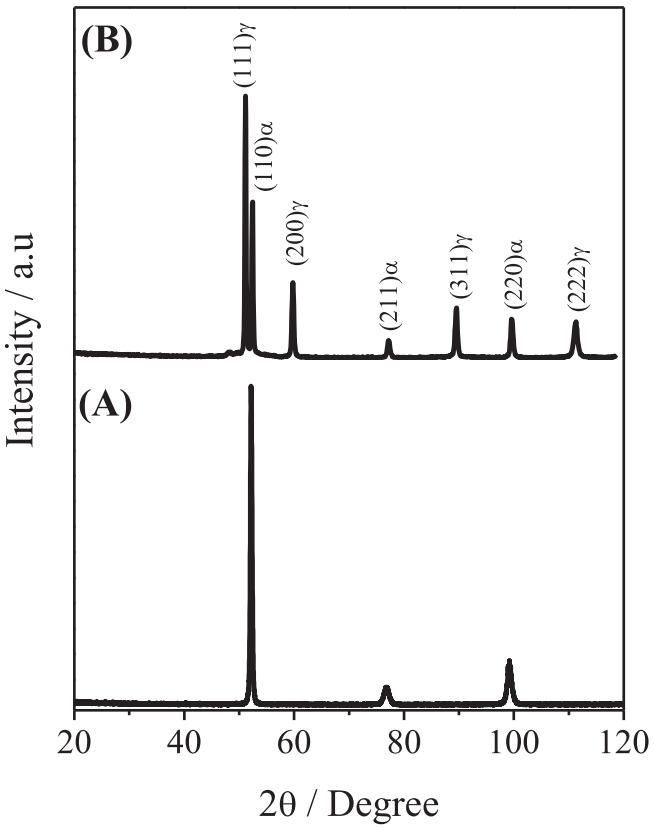


**Fig. 1.** X-ray diffractograms obtained for solution-treated (A) and aged (B) 18Ni 300 grade maraging steel samples.

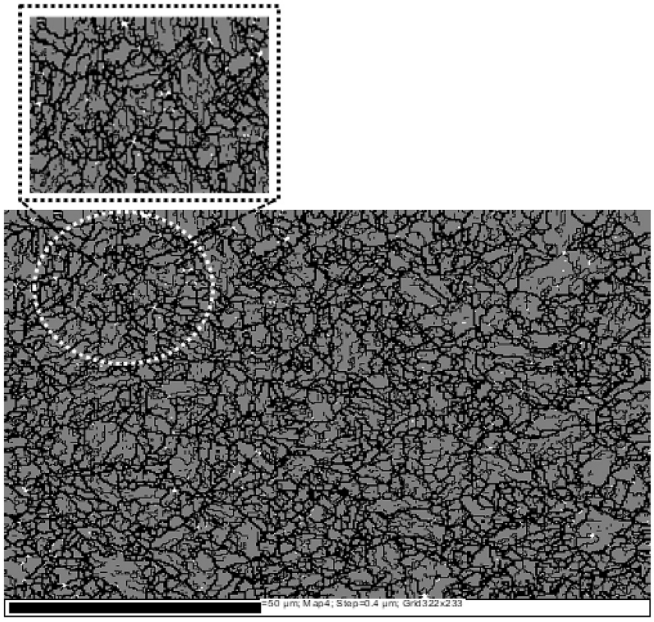

**Fig. 2.** EBSD phase map obtained for 18Ni 300 grade maraging steel aged at 650 °C for 3 h. The austenite phase is the white color and martensite phase is the gray color.

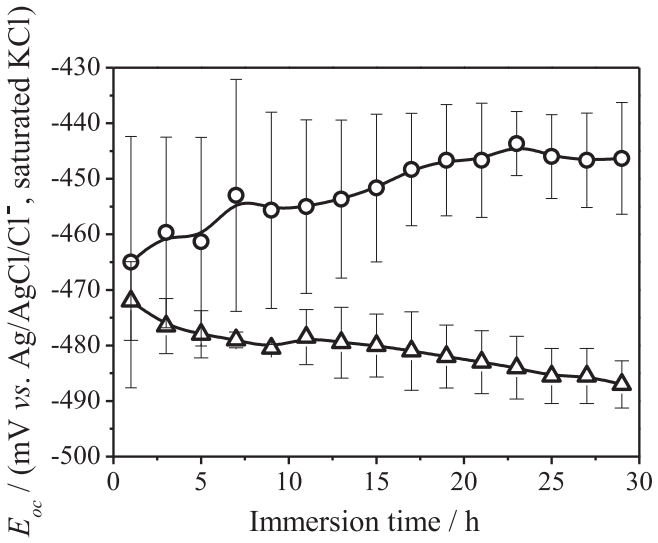


**Fig. 3.** Variation of the open circuit potential obtained for 18Ni 300 grade maraging steel with immersion time in aqueous solution containing 0.6 mol $L^{-1}$ NaCl, 1 mmol $L^{-1}$ $H_2S$ and saturated with $CO_2$ gas. The studied samples were: solution-treated at 840 °C for 1 h (O) and aged at and 650 °C (Δ) for 3 h.

### 2.2. Electrochemical corrosion tests

The electrochemical measurements were carried out by using a Metrohm AUTOLAB PGSTAT 302N potentiostat controlled by a computer using the software NOVA 11.1, which allowed the acquisition and analysis of the electrochemical data. All experiments data were performed in triplicate.

The electrochemical experiments were performed in a single-compartment Pyrex® glass cell with a Teflon cover containing holes to fix the electrodes and to allow the gas bubbling. The reference and auxiliary electrodes were the $Ag_{(s)}/AgCl_{(s)}/Cl^-_{(aq)}$ (saturated KCl) and a 2 $cm^2$ platinum plate, respectively, while the solution-treated and the aged samples were the working electrodes. The corrosion tests were carried at room temperature (about 25 °C) and using open circuit monitoring, potentiodynamic polarization and electrochemical impedance spectroscopy techniques. The polarization curves were recorded at a constant sweep rate of 1 mV $s^{-1}$ from open circuit potential ($E_{oc}$) towards more positive potentials. The impedance diagrams were obtained in the steady open circuit potential disturbed with amplitude of 10 mV peak-to-peak AC sine wave at frequencies from 20 kHz to 6 mHz.

The preparation of the testing solution followed the following steps: 0.6 mol $L^{-1}$ NaCl was dissolved in a buffered acetic acid/sodium acetate solution (pH 4.2). After, the solution was placed inside the electrochemical cell and $N_2$ gas was bubbled for 1 h to deoxygenize the solution. Next, $CO_2$ was bubbled and a mass corresponding to a $2.83 \times 10^{-4}$ mol $L^{-1}$ $Na_2S \cdot 9H_2O$ (Vetec) was dissolved only when the solution pH reached about 4.2. This amount of $Na_2S \cdot 9H_2O$ was used to have 1 mmol $L^{-1}$ $H_2S$ in solution [43]. This solution was prepared to simulate the oilfield water formation containing chloride ions, $CO_2$ and $H_2S$, since $CO_2$ and $H_2S$ are present in the oil extracted from deep ocean areas, such as the pre-salt region. Thus, the concentration of 0.6 mol $L^{-1}$ NaCl was taken to simulate the chloride concentration in sea water.

### 2.3. Characterization

X-ray diffractograms were obtained using a Panalytical diffractometer, model X-Pert PRO MPD®, in step scan mode with step size of 0.01°, time per step of 3 s and angular interval 10°–120°. Radiation CoK$\alpha$ (1.7890 Å) was used with 40 kV and 40 mA with a hybrid monochromator. The crystallographic phases were identify using the software X-pert HighScore Plus® version 3.0.5 and the crystallography data for all phases were obtained using the Inorganic Crystal Structure Database (ICSD).

The XPS data were collected using non-monochromatic Al K$\alpha$ radiation at 1486.6 eV and 152 W. A survey spectrum together with high resolution regions of C 1s, O 1s, S 2p, Fe 2p, Ni 2p, Mo 3d and Ti 2p were recorded. All binding energies used in this work were referenced to the binding energy of the carbon C 1s peak at 284.0 eV which is from the presence of adsorbed hydrocarbons. The XPS spectra were obtained for both solution-treated and aged maraging steel samples, after 29 h of immersion in aqueous solution containing 0.6 mol $L^{-1}$ NaCl, 1 mmol $L^{-1}$ $H_2S$ and saturated with $CO_2$ gas.

The investigation of the surface morphology of the 18Ni 300 grade maraging steel was carried out using a INSPECT S50-FEI scanning electron microscope (SEM) before and after the corrosion tests.

Lastly, EBSD maps were obtained in an Oxford Channel 5-EBSD system coupled to a Philips® XL-30 SEM. Sample preparation sequence was a pre-grind to 600 SiC and polished to 3, 2 and 1 μm diamond paste. The final polishing was done using a colloidal silica suspension of particle size of 0.05 μm during extended periods of time.

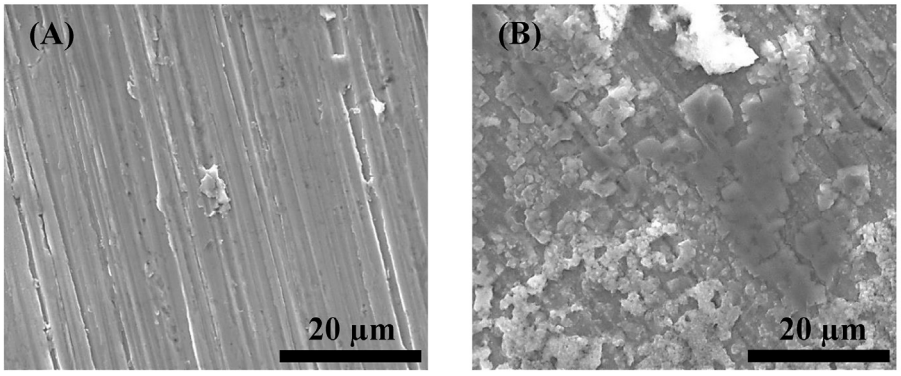


**Fig. 4.** - SEM images obtained for 18Ni 300 grade maraging steel solution-treated at (A) 840 °C for 1 h and aged at (B) 650 °C for 3 h after 29 h of immersion in aqueous solution containing 0.6 mol $L^{-1}$ NaCl, 1 mmol $L^{-1}$ $H_2S$ and saturated with $CO_2$ gas.

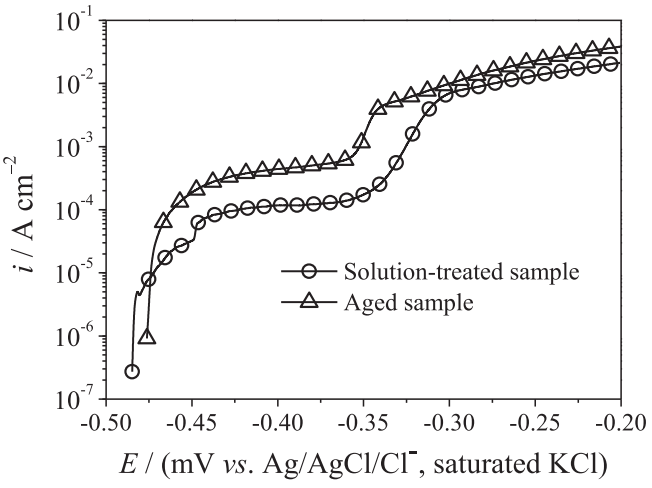


**Fig. 5. -** Anodic potentiodynamic polarization curves obtained in aqueous solution containing 0.6 mol $L^{-1}$ NaCl solution, 1 mmol $L^{-1}$ $H_2S$ aqueous and saturated with $CO_2$ gas for the 18Ni 300 grade maraging steel samples which were solution-treated at 840 °C for 1 h (O) and aged at 650 °C (Δ) for 3 h.

## 3. Results and discussion

### 3.1. X-ray diffractograms and EBSD phase map

Fig. 1 shows the X-ray diffractograms obtained for maraging steel that was solution-treated at 840 °C for 1 h (Fig. 1a) and aged at 650 °C for 3 h (Fig. 1b). The X-ray diffraction pattern shown in Fig. 1a presents three well defined peaks located at 2θ ≈ 52°, 77° and 99°, corresponding to the planes {110}, {200} and {211} from the body centered cubic martensitic matrix (α') (ICSD no. 76747). Moreover, these peaks are also detected in the diffractogram of the aged sample. Besides the peaks of the α' phase, the X-ray diffraction pattern of the aged sample (Fig. 1b) presented four well-defined characteristic peaks around 2θ ≈ 51°, 60, 90° and 112°, which are attributed to {111}, {200}, {220} and {311} set planes related to face centered cubic structure (Fig. 1b) (ICSD no. 185066) corresponding to the reverted austenite (γ) formed from the partial transformation of martensite. Finally, these results are in close agreement with others reports already published in literature [7,8]. The EBSD technique was also used to characterize the presence of austenite phase in the aged sample at 650 °C for 3 h. The obtained EBSD image, shown in Fig. 2, shows that the γ phase (white color) is

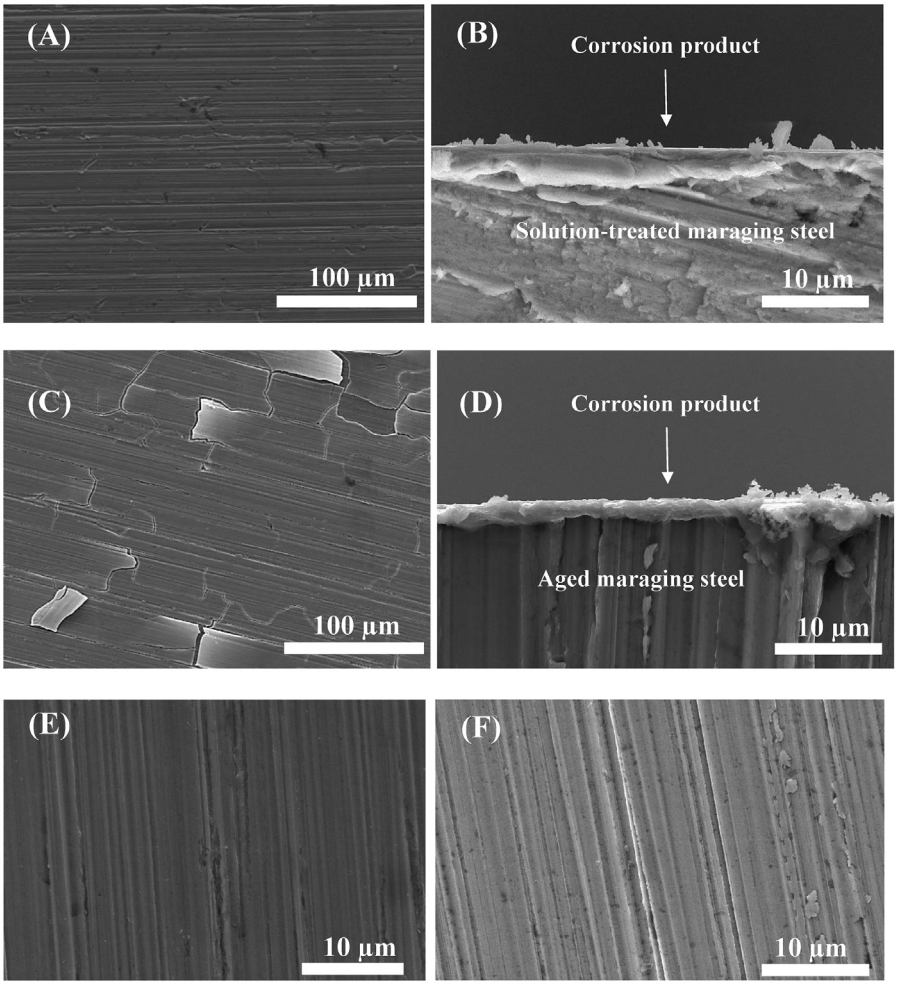


**Fig. 6.** SEM images showing the surface morphologies of the corrosion product deposited on solution-treated (A, B) and on aged (C, D) 18Ni 300 grade maraging steel samples after the end of the potentiodynamic polarization tests and carried out in aqueous solution containing 0.6 mol $L^{-1}$ NaCl solution, 1 mmol $L^{-1}$ $H_2S$ aqueous and saturated with $CO_2$ gas. Typical SEM images obtained for the surface of the solution-treated (E) and aging (F) samples, before the electrochemical corrosion tests, are also shown.

formed on the grain boundaries of the martensite matrix (gray color).

### 3.2. Electrochemical corrosion tests

The variations of the open circuit potential ($E_{oc}$) with the immersion time ($t$) for both investigated 18Ni 300 grade maraging steel samples in 0.6 mol $L^{-1}$ NaCl solution, containing 1 mmol $L^{-1}$ $H_2S$ and saturated with $CO_2$, are displayed in Fig. 3. The results were obtained in triplicate, and the error bar related to the standard deviation of the solution-treated sample showed a significant deviation in the first hours of immersion. This behavior is attributed to the differences in the surface roughness between the samples caused by sanding process. Initially, it can be noted that $E_{oc}$ values obtained for the solution-treated samples were nobler in comparison with those obtained for aged sample. Furthermore, while the $E_{oc}$ values of the solution-treated samples followed a rising tendency towards more positive potentials, the $E_{oc}$ values of the aged sample slightly shifted towards less positive potentials. The shift of the $E_{oc}$ values towards more positive potentials is related with the formation of a protective film that covered the whole surface of the solution-treated sample (visual observation). After the immersion test, the SEM examination of solution-treated sample revealed that the protective film formed on the surface of steel was homogeneous and uniform. Additionally, no cracks in this passive barrier were observed (Fig. 4A). On the other hand, the shift towards more negative potentials is associated with the formation of a non-protective film that covered the whole surface of the aged sample (visual observation) and, as revealed by the SEM image (Fig. 4B), one can observe a surface with more defects, including cracks, which made easier the penetration of the electrolyte through the film.

Thus, the analyses of Figs. 3 and 4 suggest that at $E_{oc}$ condition, a protective film was formed on the surface of the solution-treated sample and a non-protective film was deposited on the surface of the sample aged at 650 °C. Since the aging heat treatment led to the formation of the austenitic phase, the decreasing the $E_{oc}$ for less noble values, observed for the aged samples, was associated to the occurrence of the heterogeneities in the grains matrix that led to the broken of the film deposited on surface of the aged sample.

The anodic potentiodynamic polarization curves achieved for the solution-treated and for aged samples are shown in Fig. 5. Initially, it can be noted, in the entire potential range, that the current densities displayed by the solution-treated sample are lower in comparison with those obtained for the aged sample. The current plateaus observed between −440 mV and −350 mV indicate the deposition of corrosion product on alloy surfaces. For applied potentials higher than −350 mV, the current densities are rising, which is related to the dissolution of the surface film. Thus, the polarization curves show that the solution-treated sample is more corrosion resistant than the aged sample.

Fig. 6 shows the SEM images obtained to assess surface morphologies and the cross-section views of the both investigated maraging steel samples after the end of the potentiodynamic polarization tests. For the solution-treated samples (Fig. 6A), the SEM image shows an uniform film deposited on the surface with some superficial defects (Fig. 6A), while for the aged samples, the SEM image shows that the deposited film is cracked (Fig. 6C). The cross-section SEM images (Fig. 6B and D) revelled that the corrosion products deposited on both solution-treated and aged samples were uniform and cracks from the top until the bottom were not observed, indicated that the cracks, displayed in Fig. 6C, are superficial. In addition, the SEM cross-section analyses allowed the estimate the thickness of the film deposited on the both sample surface, which were about 4.54 μm and 2.10 μm for the solution-treated and aged samples, respectively, proving that the corrosion products deposited on aged sample surfaces were electrochemically less stable than those deposited on the surface of the solution-treated sample. Additionally, SEM micrographs of the surface of maraging steel at both solution-treated and aged conditions, before the potentiodynamic polarization tests, are displayed in Fig. 6E and 6F, respectively. As can be seen, before the corrosion tests, clean surfaces with sanding marks were observed.

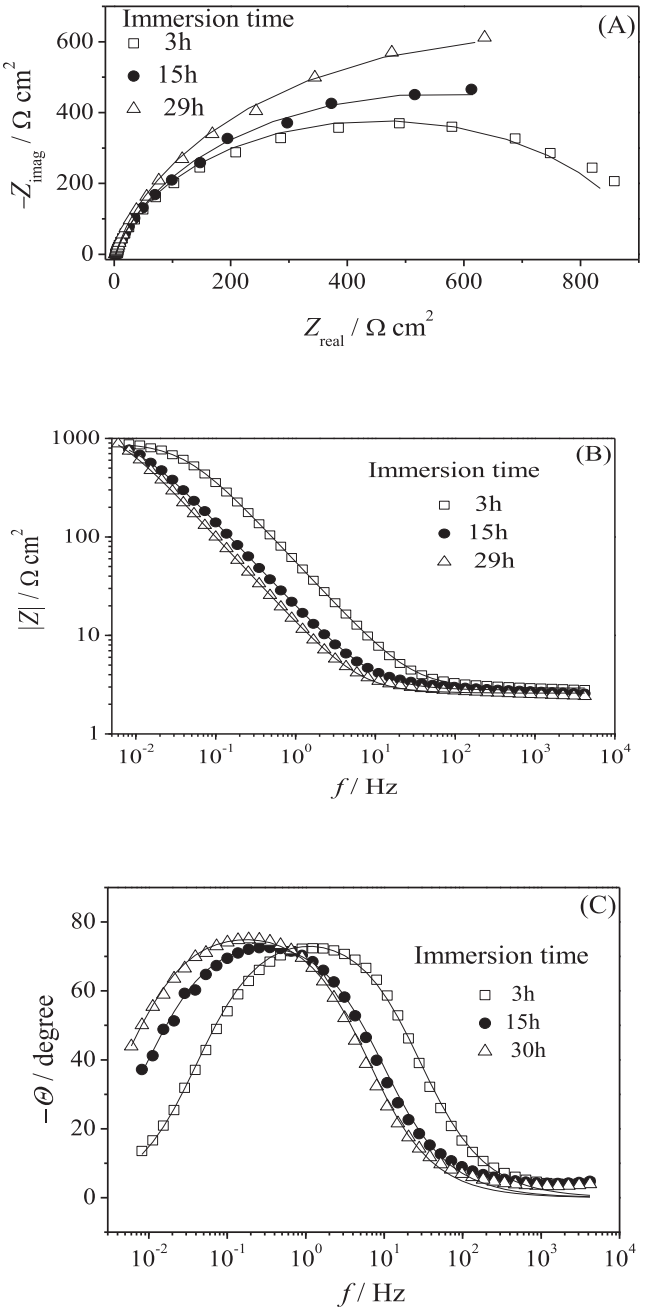


**Fig. 7.** - Typical Nyquist and Bode diagrams obtained for the solution-treated 18Ni 300 grade maraging steel samples in a 0.6 mol $L^{-1}$ NaCl solution, containing 1 mmol $L^{-1}$ $H_2S$ and saturated with $CO_2$ gas. The lines in these plots correspond to the simulated data.

The representatives Nyquist and Bode plots, obtained for solution-treated and for aged maraging steel at open circuit potential are shown in Figs. 7 and 8. Since an unique capacitive loop

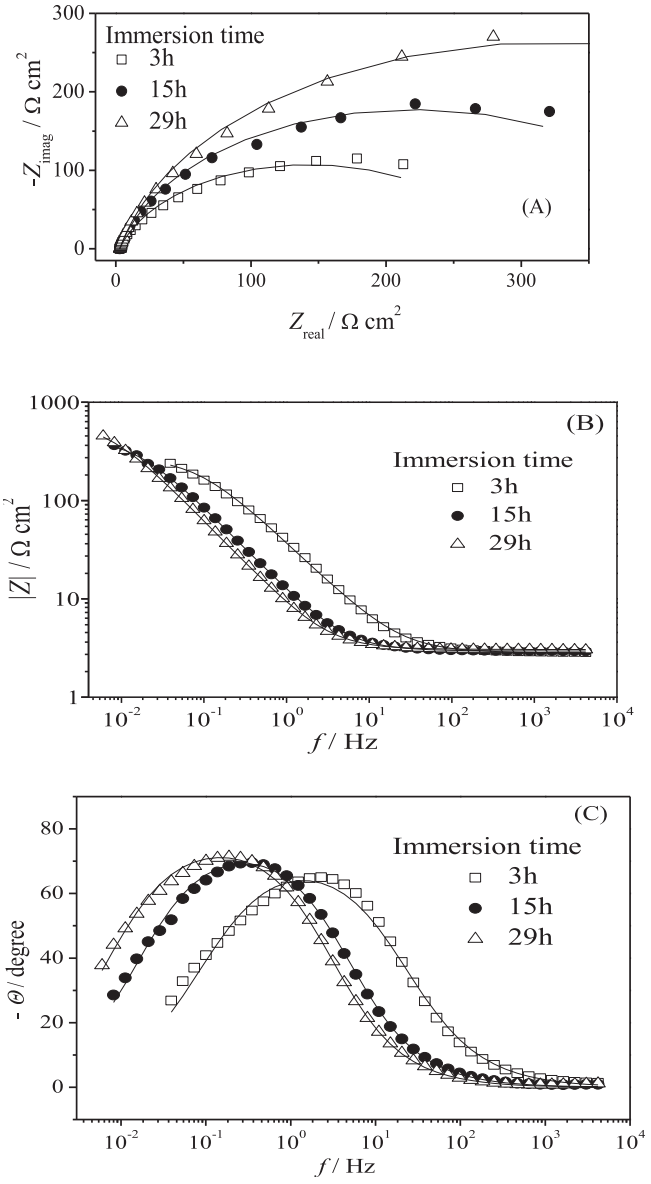


**Fig. 8.** Typical Nyquist and Bode diagrams obtained in 0.6 mol $L^{-1}$ NaCl aqueous solution, containing 1 mmol $L^{-1}$ $H_2S$ and saturated with $CO_2$ gas, for the 18Ni 300 grade maraging steel samples aged at 650 °C for 3 h. The lines in these plots correspond to the simulated data.

was observed in all obtained impedance diagrams, the experimental impedance data (symbols in Figs. 7 and 8) were fitted by equivalent electric circuit shown in Fig. 9. The observed capacitive loop is associated to the electron transfer reaction occurring at electrode/solution interface.

In Fig. 9, $R_s$ is the solution resistance, $R_{ct}$ is the charge transfer resistance and Q is the constant phase element (CPE), which is related to the capacitance or resistance of the electric double layer at electrode/solution interface. The solid lines in Figs. 7 and 8 correspond to the overlayed curve obtained by equivalent circuit analysis obtained by NOVA® software. Equation (1) was applied to convert the CPE to pseudo capacitance ($C_{pseudo}$).

$$C_{pseudo} = \sqrt[n]{\frac{Y_0}{R_{ct}^{n-1}}} \quad (1)$$

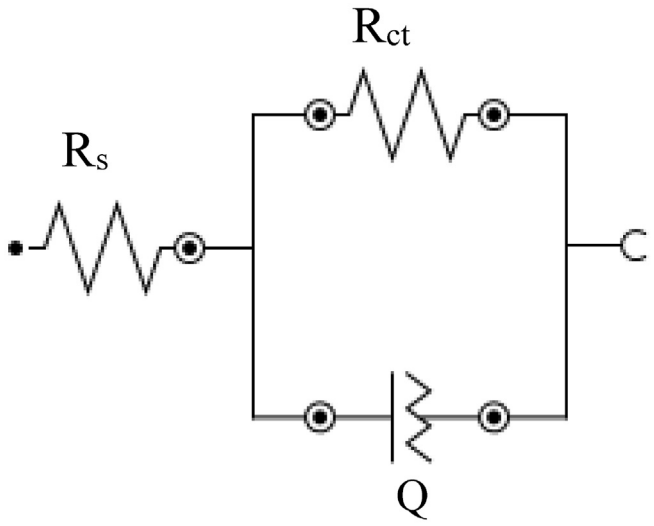


**Fig. 9.** Electric circuit used to fit the experimental electrochemical impedance diagrams.

In this equation, $Y_0$ is the admittance value of the constant phase element and $n$ is the fitted exponential of the CPE. The average values of all electric impedance parameters using the equivalent circuit for 18Ni 300 grade maraging steel in both solution-treated and aged conditions are listed in Tables 2 and 3, respectively. Both tables showed that the obtained values of $R_{ct}$ and $C_{pseudo}$ increases with the immersion time for the maraging steel in both heat-treatment conditions. Previous reports [48,49] pointed out that the increases of $R_{ct}$ and $C_{pseudo}$ values with the immersion time are related to the improvement of the barrier properties due to the film deposited on the surface of steel and to the water and ions uptake through the micropores and defects of the deposited films, respectively. During the entire duration of the immersion tests, the solution-treated samples always displayed higher $R_{ct}$ and lower $C_{pseudo}$ values in comparison with the corresponding values obtained for the aged material. Thus, the obtained impedance data suggest that the film deposited on aged sample is less protective than that deposited on solution-treated sample, which is corroborated by the SEM images shown in Fig. 4, since, after the end of the immersion tests, the film deposited on aged samples present more defects, making this film less protective and allowing permeation of water be easier.

Finally, a comparison between the $R_{ct}$ values obtained for the solution-treated and aged 18Ni 300 grade maraging steel with those recorded for carbon steel is given in Table 4. As can be seen in this table, the charge transfer resistance of maraging steel is higher than carbon steel in both heat-treated conditions investigated. After 3 h of immersion, the $R_{ct}$ values of solution-treated steel is around twice than the carbon steel, moreover, these difference increase with the immersion time. The charge transfer resistance of solution-treated maraging steel become about ten times higher than carbon steel after 23 h of immersion.

### 3.3. XPS analysis

XPS analyses were performed to obtain information about the chemical nature of films deposited on surface of both solution-treated and aged samples surfaces after 30 h of immersion in 0.6 mol $L^{-1}$ NaCl solution containing 1 mmol $L^{-1}$ $H_2S$ and saturated with $CO_2$ medium. The high resolution XPS spectra were obtained from deconvolution of peaks in the C 1s, O 1s, S 2p, Fe 2p, Ni 2p, Mo

**Table 2**
Electric circuit parameters calculated from the adjust of the impedance spectra obtained for the solution-treated 18Ni 300-grade maraging steel samples in 0.6 mol $L^{-1}$ NaCl aqueous solution, containing 1 $mmol^{-1}$ $H_2S$ and saturated with $CO_2$ gas. The listed values correspond to the average value of three replicates.

| Immersion Time/h | $R_s/\Omega\ cm^2$ | $R_{ct}/\Omega\ cm^2$ | $C_{pseudo}/mF\ cm^{-2}$ | $\chi^2/\times10^{-3}$ |
|---|---|---|---|---|
| 3 | 2.50 (±0.65) | 715.8 (±230.6) | 3.51 (±2.54 × $10^{-4}$) | 12.6 |
| 5 | 2.50 (±0.68) | 905.2 (±275.5) | 5.40 (±1.03 × $10^{-4}$) | 11.7 |
| 7 | 2.50 (±0.58) | 989.1 (±71.91) | 7.22 (±2.32 × $10^{-4}$) | 18.2 |
| 9 | 2.60 (±0.58) | 1199.4 (±283.7) | 8.93 (±3.93 × $10^{-4}$) | 9.86 |
| 11 | 2.60 (±0.57) | 1265.0 (±371.9) | 9.42 (±1.66 × $10^{-4}$) | 9.04 |
| 13 | 2.60 (±0.49) | 1420.7 (±570.3) | 11.50 (±6.76 × $10^{-4}$) | 11.3 |
| 15 | 2.70 (±0.40) | 1619.5 (±719.1) | 12.80 (±9.12 × $10^{-4}$) | 10.9 |
| 17 | 2.80 (±0.44) | 1845.5 (±852.0) | 13.61 (±9.40 × $10^{-4}$) | 8.93 |
| 19 | 2.80 (±0.29) | 2083.5 (±1126.4) | 14.48 (±10.80 × $10^{-4}$) | 12.7 |
| 21 | 2.90 (±0.30) | 2144.5 (±1119.3) | 15.14 (±11.46 × $10^{-4}$) | 10.2 |
| 23 | 2.90 (±0.17) | 2137.5 (±1140.6) | 16.30 (±13.00 × $10^{-4}$) | 10.2 |
| 25 | 2.80 (±0.09) | 2040.5 (±1096.7) | 17.00 (±14.50 × $10^{-4}$) | 4.85 |
| 27 | 2.80 (±0.05) | 2042.5 (±1037.3) | 17.70 (±15.92 × $10^{-4}$) | 5.25 |
| 29 | 2.80 (±0.01) | 2096.0 (±973.0) | 18.50 (±16.60 × $10^{-4}$) | 6.45 |

**Table 3**
Electric circuit parameters calculated from the adjust of the impedance spectra obtained for the aged 18Ni 300-grade maraging steel samples in 0.6 mol $L^{-1}$ NaCl aqueous solution, containing 1 $mmol^{-1}$ $H_2S$ and saturated with $CO_2$ gas. The listed values correspond to the average value of three replicates.

| Immersion Time/h | $R_s/\Omega\ cm^2$ | $R_{ct}/\Omega\ cm^2$ | $C_{pseudo}/mF\ cm^{-2}$ | $\chi^2/\times10^{-3}$ |
|---|---|---|---|---|
| 3 | 2.50 (±0.01) | 285.5 (±55.4) | 7.75 (±8.75 × $10^{-4}$) | 38.9 |
| 5 | 2.60 (±0.15) | 318.7 (±42.6) | 12.1 (±5.63 × $10^{-4}$) | 19.4 |
| 7 | 2.70 (±0.19) | 362.7 (±18.3) | 15.0 (±5.00 × $10^{-4}$) | 11.9 |
| 9 | 2.70 (±0.21) | 402.7 (±22.0) | 16.9 (±5.48 × $10^{-4}$) | 9.40 |
| 11 | 2.70 (±0.22) | 413.6 (±51.3) | 19.2 (±1.17 × $10^{-4}$) | 8.10 |
| 13 | 2.70 (±0.27) | 450.8 (±70.2) | 21.0 (±1.51 × $10^{-4}$) | 9.65 |
| 15 | 2.70 (±0.30) | 477.0 (±52.0) | 22.7 (±5.07 × $10^{-4}$) | 9.55 |
| 17 | 2.80 (±0.35) | 515.3 (±46.0) | 24.4 (±8.20 × $10^{-4}$) | 11.0 |
| 19 | 2.80 (±0.33) | 537.2 (±55.4) | 26.4 (±11.40 × $10^{-4}$) | 15.0 |
| 21 | 2.80 (±0.34) | 564.1 (±45.3) | 28.1 (±11.46 × $10^{-4}$) | 14.5 |
| 23 | 2.80 (±0.37) | 589.6 (±40.4) | 29.4 (±13.5 × $10^{-4}$) | 16.0 |
| 25 | 2.80 (±0.39) | 625.5 (±45.6) | 30.8 (±14.4 × $10^{-4}$) | 18.6 |
| 27 | 2.80 (±0.40) | 645.3 (±47.2) | 32.3 (±17.2 × $10^{-4}$) | 22.0 |
| 29 | 2.80 (±0.40) | 671.3 (±43.1) | 33.1 (±18.0 × $10^{-4}$) | 24.0 |

3d and Ti 2p regions for both solution-treated and aged samples were very similar and shown in Figs. 10–16.

The typical obtained C1s XPS spectrum is displayed in Fig. 10. This figure shows three deconvoluted peaks. The first peak, located at 284.8 eV, is attributed to C-C and C-H groups present in the hydrocarbon adsorbed on film surface. Unfortunately, it is not possible to state the source of the measured C signal, since, before the XPS measurements, the samples were washed, dried, and exposed to air. The second peak is positioned at 286.4 eV and it is associated to carbon bonded to oxygen, such as C-O, C-OH. The third peak, positioned at 288.4 eV, correspond to carbon in the carbonate [42,50].

**Table 4**
Comparison between the $R_{ct}$ values obtained for the solution-treated and aged 18Ni 300 grade maraging steel, in this investigation, and those reported in the literature for other alloys materials.

| N° | Ref. | Material | Solution | Temperature/°C | pH | Immersion time/h | $R_{ct}/\Omega\ cm^2$ |
|---|---|---|---|---|---|---|---|
| 1 | Choi et al. [24] | Carbon steel (AISI C1018) | 1 wt% NaCl containing 100 ppm $H_2S$ and 0.097 MPa $CO_2$ | 25 | 3.0 | 2 | ≈250[a] |
| 2 | Choi et al. [24] | Carbon steel (AISI C1018) | 1 wt% NaCl containing 100 ppm $H_2S$ and 0.097 MPa $CO_2$ | 25 | 3.0 | 2 | ≈250[a] |
| 3 | Yu et al. [26] | Low alloy steel | 3.5 wt% NaCl containing $H_2S$ and $CO_2$ | 75 | 4.2 | 24 | ≈261 |
| 4 | Abelev et al. [27] | Iron (99.98%) | 3.0 wt% NaCl containing 500 ppm $H_2S$ and $CO_2$ saturated | Room temperature | – | 1 | ≈600[a] |
| 5 | Wang et al. [31] | Low alloy steel | 3.5 wt% NaCl containing $H_2S$, $CO_2$ and $N_2$ (1:7:5) | 75 | 4.2 | 24 | ≈151.6 |
| 6 | Zimer et al. [43] | Carbon steel (AISI 1040) | 3.5 wt% NaCl containing 100 ppm $H_2S$ | Room temperature | 3.5 | 1 | ≈386.2 |
| 7 | Zimer et al. [43] | Carbon steel (AISI 1040) | 3.5 wt% NaCl containing 1000 ppm $H_2S$ | Room temperature | 3.5 | 1 | ≈489.9 |
| 8 | This work | Solution-treated maraging steel grade 300 | 3.5 wt% NaCl containing 1 mmol $L^{-1}$ $H_2S$ and $CO_2$ saturated | 25 | 4.2 | 3 | ≈715.8 |
| 9 | This work | Aged maraging steel grade 300 | 3.5 wt% NaCl containing 1 mmol $L^{-1}$ $H_2S$ and $CO_2$ saturated | 25 | 4.2 | 3 | ≈285.5.8 |
| 10 | This work | Solution-treated maraging steel grade 300 | 3.5 wt% NaCl containing 1 mmol $L^{-1}$ $H_2S$ and $CO_2$ saturated | 25 | 4.2 | 23 | ≈2037.5 |
| 11 | This work | Aged maraging steel grade 300 | 3.5 wt% NaCl containing 1 mmol $L^{-1}$ $H_2S$ and $CO_2$ saturated | 25 | 4.2 | 23.0 | ≈586.9 |

[a] This value was obtained from extrapolation of the capacitive arc to the real impedance axis, at low frequency range, and that it is displayed in the cited reference.

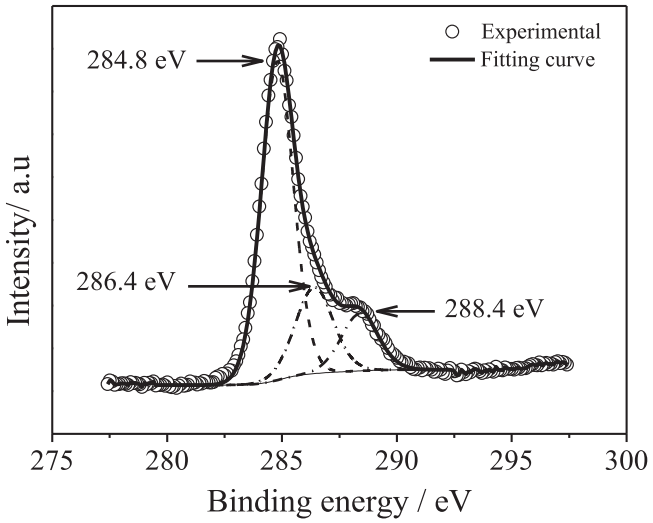


**Fig. 10.** Typical C 1s XPS spectrum obtained for the solution-treated and aged 18Ni 300 grade maraging steel samples, after 30 h of immersion in 0.6 mol $L^{-1}$ NaCl solution containing 1 mmol $L^{-1}$ $H_2S$ and saturated with $CO_2$.

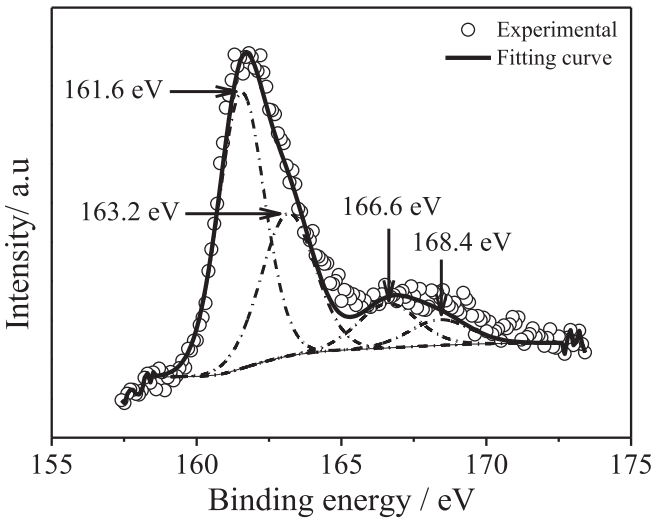


**Fig. 12.** S2p XPS spectra obtained for the solution-treated and aged 18Ni 300 grade maraging steel samples, after 30 h of immersion in 0.6 mol $L^{-1}$ NaCl solution containing 1 mmol $L^{-1}$ $H_2S$ and saturated with $CO_2$.

The typical obtained O1s XPS spectra are shown in Fig. 11. The spectra obtained for the surface films deposited on both solution-treated and aged 18Ni 300 grade maraging steel display peaks at 530.0, 531.5 and 533.2 eV, which are associated to $O^{2-}$ chemically bonding to metal ions, $O^{2-}$ chemically bonding to carbon and adsorbed water [42,50–52], respectively.

The typical obtained S2p XPS spectrum is shown in Fig. 12. Four deconvoluted peaks are shown and they are located at about 161.6, 163.2, 166.6 and 168.4 eV. The peak at about 161.6 eV is related to the presence of sulphide ($S^{2-}$) [53–59], and that located at 163.2 eV was attributed to disulphide ($S_2^{2-}$) [27,57–59]. The peaks observed at about 166.6 eV and 168.4 eV are associated to the sulphate ($SO_4^{2-}$) [57,59]. Therefore, the analysis of the S2p XPS spectra suggests that sulphide, disulphide and sulphates compounds were present in the film deposited on the surface of both investigated maraging steel samples.

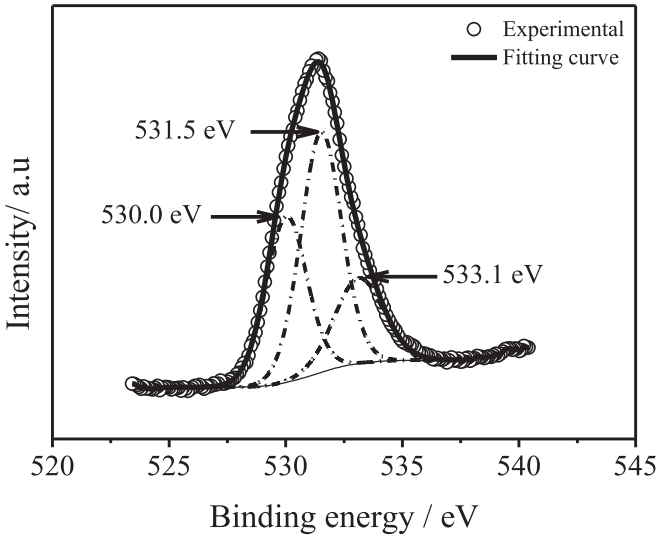


**Fig. 11.** O1s XPS spectra obtained for the solution-treated and aged 18Ni 300 grade maraging steel samples, after 30 h of immersion in 0.6 mol $L^{-1}$ NaCl solution containing 1 mmol $L^{-1}$ $H_2S$ and saturated with $CO_2$.

The typical Fe2p 3/2 XPS spectrum obtained for the corrosion products deposited on both investigated maraging steel surfaces is shown in Fig. 13. The peaks positioned at 710.7 eV and at 712.6 eV are related to the $Fe^{2+}$ chemically bonded to $CO_3^{2-}$ [42], or to $S^{2-}$ [60]. In addition, these peaks can also be assigned to the $Fe^{3+}$ bonded to $O^{2-}$ [27,42,50,51,61] species. The peaks with the binding energies of 719.2, 723.5 and 725.4 eV are also related to the $Fe^{3+}$ bonded to $O^{2-}$ [27,42,50,51,60] species.

Thus, the association of the peaks positioned at 286.4 eV in the C1s XPS (Fig. 10), at 530.0, 531.5 and 533.2 eV in the O1s spectra (Fig. 11) and the peaks at 710.7, 719.2, 712.6, 723.5 and 725.4 eV, indicates the presence of $FeCO_3$ in corrosion products. Another association that can be made is between the peaks at 530.0 eV, in O1s XPS spectrum (Fig. 11) and the peaks at 710.7, 719.2, 712.6, 723.5 and 725.4 eV in Fe2p spectrum (Fig. 13), suggesting the presence of $Fe_2O_3$ in the corrosion products [37,43,44]. Finally, the association of the peaks positioned at 161.6 eV, at 166.6 eV and at 168.4 eV, in S2p XPS spectrum (Fig. 12), with that located at 712.6 eV, in the Fe2P XPS spectrum (Fig. 13), suggesting the formation of FeS and $FeSO_4$.

Fig. 14 shows the typical Ni2p XPS spectra obtained for the as-solution-treated and aged maraging steel samples. Six well defined peaks at 852.6, 855.4, 861.3, 870.1, 873.0 and 879.1 eV are shown in Fig. 14. The peak positioned at 852.6 eV is associated to metallic nickel [62–66], which is due to the steel substrate. The peaks positioned at 855.4, 861.3, and 879.1 eV were related to $Ni^{2+}$ bonded with $S^{2-}$ [60,64,66], while the peaks with binding energies at 861.3 and 873.0 eV can be associated to $Ni^{2+}$ bonding with $O^{2-}$, or $SO_4^{2-}$, or $OH^-$ [64]. Thus, the analysis of the Ni2p XPS suggests that NiS, $NiSO_4$, $Ni(OH)_2$ and NiO are present in the corrosion layer deposited on both maraging steel samples.

Fig. 15 shows the Mo3d XPS spectra achieved for the corrosion products deposited on solution-treated (Fig. 15A) and aged maraging steel (Fig. 15B) samples. In Fig. 15A, the peak that appears at about 226.4 eV is very close to that observed at 226 eV in the XPS spectrum of amorphous molybdenum sulfide quantum dots by Dinda et al. [67] and, therefore, this peak observed at 226.4 eV is associated to the presence of $MoS_2$ in the film deposited on the surface of the solution-treated sample. Two peaks are displayed at 232.2 eV and at 235.2 eV and they are related to the $Mo^{6+}$ forming

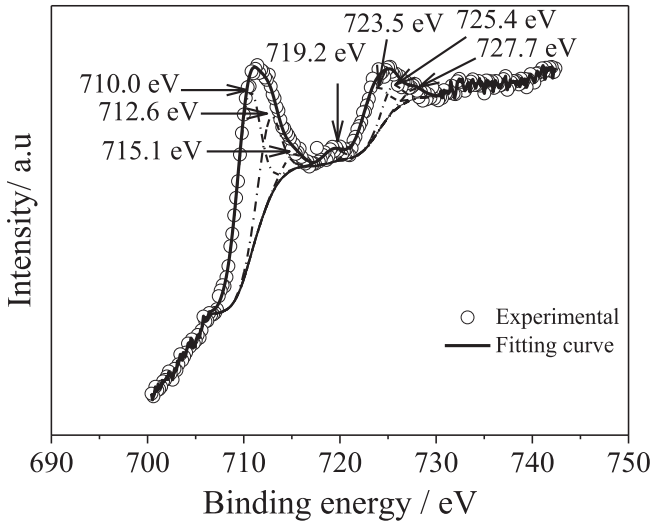


**Fig. 13.** Fe 2p XPs spectra obtained for the solution-treated and aged 18Ni 300 grade maraging steel samples, after 30 h of immersion in 0.6 mol $L^{-1}$ containing 1 mmol $L^{-1}$ $H_2S$ and saturated with $CO_2$.

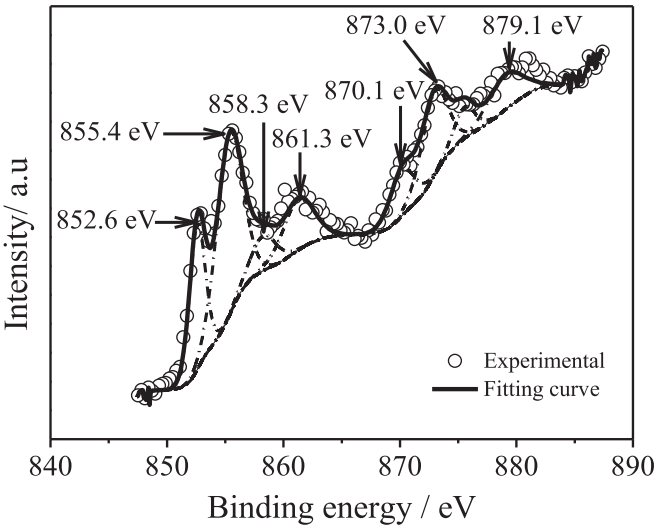


**Fig. 14.** Ni 2p XPs spectra obtained for the solution-treated and aged 18Ni 300 grade maraging steel samples, after 30 h of immersion in 0.6 mol $L^{-1}$ containing 1 mmol $L^{-1}$ $H_2S$ and saturated with $CO_2$.

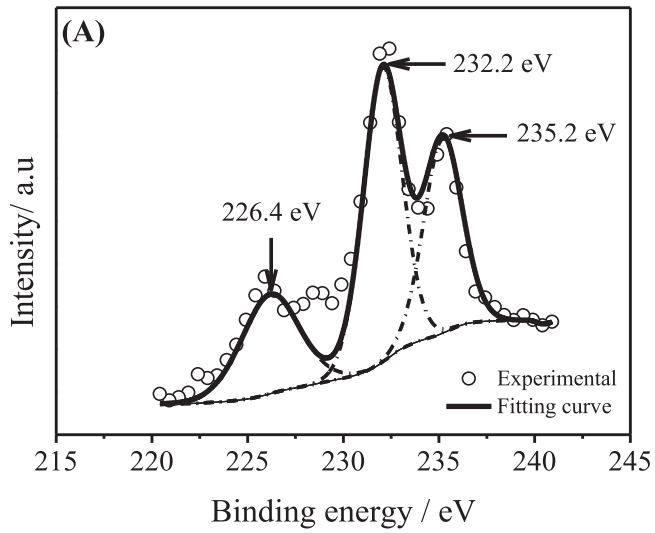


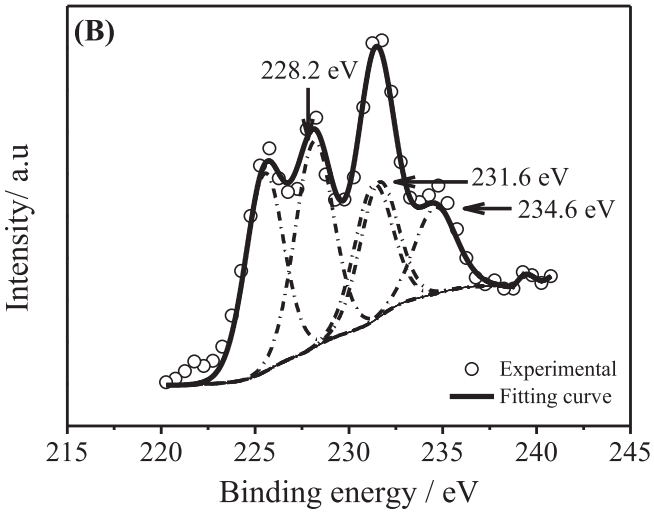


**Fig. 15.** Mo3d XPS spectra obtained for the solution-treated (A) and aged (B) 18Ni 300 grade maraging steel samples, after 30 h of immersion in 0.6 mol $L^{-1}$ containing 1 mmol $L^{-1}$ $H_2S$ and saturated with $CO_2$.

chemical bonding with $O^{2-}$ [68–70]. Therefore, the analysis Mo3d XPS spectrum, obtained for the solution-treated maraging steel (Fig. 15A), indicates that $MoS_2$ and $MoO_3$ are present in the corrosion products deposited on solution-treated maraging steel sample. On the other hand, four peaks can be observed in the XPS spectrum displayed in Fig. 15B. The peak located at 228.2 eV is related to the $Mo^{4+}$ in $MoO_2$ and in $MoS_2$, while the others two peaks at 231.6 and 234.6 eV correspond to the $MoO_3$. Thus, the XPS spectrum, obtained for aged sample, suggest the $MoO_2$, $MoS_2$ and $MoO_3$ were formed on aged sample surface during the immersion test.

Finally, the Ti2p XPs spectra obtained for both studied maraging samples were similar and that obtained for the solution-treated sample is shown in Fig. 16. Two well defined peaks located at 458.5 and 463.5 eV are displayed in this spectrum and they are related to the presence of $TiO_2$ [62], indicating this oxide was present in the corrosion products deposited on surface of both solution-treated and aged maraging steel.

## 4. Conclusions

Solution-annealed and aging 18Ni 300 grade maraging steel samples were successful obtained at 840 °C, for 1 h, and at 650 °C, for 3 h, respectively. X-ray diffraction and EDSB techniques evidenced the formation of austenitic phase due to the aging heat treatment. Among the investigated samples, the aged presented the worst corrosion resistance performance in 0.6 mol $L^{-1}$ NaCl solution, containing 1 mmol $L^{-1}$ $H_2S$ and saturated with $CO_2$. Therefore, the electrochemical results indicated that the formation of the austenitic phase was deleterious for the corrosion resistance of the investigated maraging steel. SEM images made possible to characterize the deposition of corrosion products on the surface of

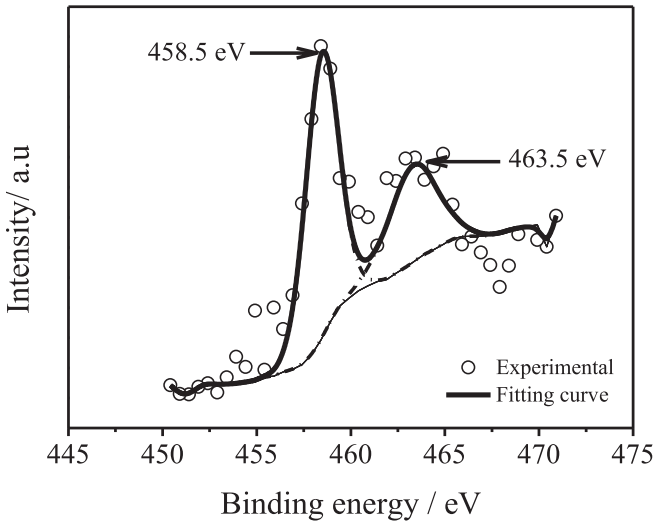


**Fig. 16.** Typical Ti 2p XPs spectrum obtained for the solution-treated and aged 18Ni 300 grade maraging steel samples, after 30 h of immersion in 0.6 mol $L^{-1}$ containing 1 mmol $L^{-1}$ $H_2S$ and saturated with $CO_2$.

both maraging steel samples after the end of immersion assays and potentiodynamic polarization experiments. In addition, XPS spectra suggested that the deposited films were composed by $FeCO_3$, $Fe_2O_3$, $FeS_2$, $FeSO_4$, NiO, $Ni(OH)_2$, NiS, $NiSO_4$, $MoO_2$, $MoO_3$ and $MoS_2$ compounds. Finally, the investigation showed that for an industrial application that requires the corrosion resistance property of the 18Ni 300 grade maraging steel, it must be thermal solution-treated before its use.

## Acknowledgements

The authors gratefully acknowledge the CNPq, CAPES, FINEP and FUNCAP (Brazil) for financial assistance. The authors would like to thank the Central Analítica-UFC/CT-INFRA/MCTI-SISNANO/Pró-Equipamentos CAPES, Characterizations Laboratory-UFC and the X-Ray Laboratory-UFC (Project: 402561/2007-4 (Edital MCT/CNPq nº 10/2007) for technical support.

## References

[1] S. Floreen, The physical metallurgy of maraging steels, Inter. Mater. Rev. 13 (1968) 115.
[2] W. Sha, A. Cerezo, G.D.W. Smith, Atom probe studies of early stages of precipitation reactions in maraging steels I. Co- and Ti-containing C-300 steel, Scr. Metall. Mater. 26 (1992) 517. http://www.sciencedirect.com/science/journal/0956716X.
[3] W. Sha, A. Cerezo, G.D.W. Smith, Phase chemistry and precipitation reactions in maraging steels: Part I. Introduction and study of Co-containing C-300 steel, Metall. Trans. 24 (1993) 1221.
[4] R. Tewari, S. Mazumder, I.S. Batra, G.K. Dey, S. Banerjee, Precipitation in 18wt% Ni maraging steel of grade 350, Acta Mater. 48 (2000) 1187.
[5] O. Moshka, M. Pinkas, E. Brosh, V. Ezersky, L. Meshi, Addressing the issue of precipitates in maraging steels – unambiguous answer, Mater. Sci. Eng. A 638 (2015) 232.
[6] M. Farooque, H. Ayub, A.U. Haq, A.Q. Khan, The formation of reverted austenite in 18% Ni 350 grade maraging steel, J. Mater. Sci. 33 (1998) 2927.
[7] J.M. Pardal, S.S.M. Tavares, M.P. Cindra Fonseca, H.F.G. Abreu, J.J.M. Silva, Study of the austenite quantification by X-ray diffraction in the 18Ni-Co-Mo-Ti maraging 300 steel, J. Mater. Sci. 41 (2006) 2301.
[8] J.M. Pardal, S.S.M. Tavares, M.P. Cindra Fonseca, M.R. da Silva, J.M. Neto, H.F.G. Abreu, Influence of temperature and aging time on hardness and magnetic properties of the maraging steel grade 300, J. Mater. Sci. 42 (2006) 2276.
[9] G. Bellanger, J.J. Rameau, Effect of slightly acid pH with or without chloride in radioactive water on the corrosion of maraging steel, J. Nucl. Mater. 228 (1996) 24.
[10] T. Poornima, J. Nayak, A.N. Shetty, Corrosion of aged and annealed 18 Ni 250 grade maraging steel in phosphoric acid medium, J. Electrochem. Sci. 5 (2010) 56.
[11] P. Kumar, A.N. Shetty, Electrochemical investigation on the corrosion of 18%Ni M250 grade maraging steel under welded condition in sulfuric acid medium, Surf. Eng. Appl. Electrochem. 49 (2013) 253.
[12] F. Rosalbino, G. Scavino, Corrosion inhibition of high strength maraging steel by cerium (III) ions in sulfuric acid solution, Mater. Corrosion 66 (2015) 1263.
[13] P. Kumar, A.N. Shetty, Inhibition effect of adsorption layer of 1-phenyl-4-(4-nitrophenyl) thiosemicarbazide on the corrosion of 18Ni 250-grade welded maraging steel in 1.0 M hydrochloric acid medium, Res. Chem. Intermed. 41 (2015) 7095.
[14] E.S.M. Sherif, Corrosion inhibition in 2.0 M sulfuric acid solutions of high strength maraging steel by aminophenyl tetrazole as a corrosion inhibitor, Appl. Surf. Sci. 292 (2014) 190.
[15] E.S.M. Sherif, A.H. Seikh, Effects of immersion time and 5-phenyl-1H-tetrazole on the corrosion and corrosion mitigation of cobalt free maraging steel in 0.5 M sulfuric acid pickling solutions, J. Chem. (2013) 1.
[16] B.S. Sanatkumar, J. Nayak, A.N. Shetty, The corrosion inhibition of maraging steel under weld aged condition by 1(2E)-1-(4-aminophenyl)-3-(2-thienyl) prop-2-en-1-one in 1.5 M hydrochloric acid medium, J. Coating Technol. Res. 9 (2012) 483.
[17] T. Poornima, J. Nayak, A.N. Shetty, Effect of 4-(N,N-diethylamino)benzaldehyde thiosemicarbazone on the corrosion of aged 18 Ni 250 grade maraging steel in phosphoric acid solution, Corrosion Sci. 53 (2011) 3688.
[18] L.P.M. Santos, M. Béreš, I.N. Bastos, S.S.M. Tavares, H.F.G. Abreu, M.J.G. da Silva, Hydrogen embrittlement of ultra high strength 300 grade maraging steel, Corrosion Sci. 101 (2015) 12.
[19] S.K. Manwatkar, S.V.S.N. Murty, P.R. Narayanan, S.C. Sharma, P.V. Venkitakrishnan, Stress corrosion cracking of a maraging steel shear bolt used in the interstage structure of a satellite launch vehicle, Metallogr. Microstruct. Anal. 5 (2016) 411.
[20] A.H. Seikh, H. Halfa, M. Baig, S.M.A. Khan, Microstructure characterization and corrosion resistance behavior of new cobalt-free maraging steel produced through ESR techniques, J. Mater. Eng. Perform. 26 (2017) 1589.
[21] J. Tian, W. Wang, M.B. Shahzad, W. Yan, Y. Shan, Z. Jiang, K. Yang, A new maraging stainless steel with excellent strength–toughness–corrosion synergy, Materials 10 (2017) 1293–1304.
[22] S.D. Meshrama, A.G. Paradkara, G.M. Reddya, S. Pandey, Friction stir welding: an alternative to fusion welding for better stress corrosion cracking resistance of maraging steel, J. Manuf. Process. 25 (2017) 94.
[23] G.X. Zhao, L.X.H. Lu, J.M. Xiang, Y. Han, Formation characteristic of $CO_2$ corrosion product layer of P110 steel investigated by SEM and electrochemical technique, Iron Steel Res. Inter. 16 (2009) 89.
[24] Y.S. Choi, S. Nesic, Shiun Ling, Effect of $H_2S$ on the $CO_2$ corrosion of carbon steel in acidic solutions, Electrochim. Acta 56 (2011) 1752.
[25] Y. Zheng, B. Brown, S. Nešić, Electrochemical study and modeling of $H_2S$ corrosion of mild steel, Corrosion 70 (2014) 351–364.
[26] C. Yu, P. Wang, X. Gao, Corrosion behavior and kinetics of early stages of low alloy steel under $H_2S/CO_2$ environment, Int. J. Electrochem. Sci. 10 (2015) 6820.
[27] E. Abelev, T.A. Ramanarayanan, S.L. Bernasekz, Iron corrosion in $CO_2$/brine at low $H_2S$ concentrations: an electrochemical and surface science study, J. Electrochem. Sci. 156 (2009) 331.
[28] W. Sun, S. Nešić, S. Papavinasam, Kinetics of corrosion layer formation. Part 2-iron sulfide and mixed iron sulfide/carbonate layers in carbon dioxide/hydrogen sulfide, Corrosion 64 (2008) 586.
[29] G.C. Edward, W.B. Wright, Corrosion of iron in an $H_2S$-$CO_2$-$H_2O$ system mechanism of sulfide film formation and kinetics of corrosion reaction, Corrosion 21 (1965) 245.
[30] H. Vedage, T.A. Ramanarayanan, J.D. Mumford, S.N. Smith, Electrochemical growth of iron sulfide films in $H_2S$-saturated chloride media, Corrosion 49 (1993) 114.
[31] H. Wang, P. Zhou, S. Huang, C. Yu, Corrosion mechanism of low alloy steel in NaCl solution with $CO_2$ and $H_2S$, Int. J. Electrochem. Sci. 11 (2016) 1293.
[32] H. Maa, X. Chenga, G. Lib, S.C.Z. Quana, S. Zhaoa, L. Niu, The influence of hydrogen sulfide on corrosion of iron under different conditions, Corrosion Sci. 42 (2000) 1669.
[33] B. Brown, S. Nešić, $CO_2/H_2S$ Corrosion under Scale Forming Conditions, Corros. NACE, 2005, p. 3.
[34] G.V. Chilingar, R. Mourhatch, G. Al-Qahtani, The Fundamentals of Corrosion and Scalling - a Handbook for Petroleum and Environmental Engineers, Gulf Publishing Company, Houston, 2008.
[35] Z. Yin, W. Zhao, Z. Bai, Y. Feng, Characteristics of $CO_2$ corrosion scale formed on P110 steel in simulant solution with saturated $CO_2$, Surf. Interface Anal. 40 (2008) 1231.
[36] B. Linter, G. Burstein, Reactions of pipeline steels in carbon dioxide solutions, Corrosion Sci. 41 (1999) 117.
[37] S. Guo, L. Xu, L. Zhang, W. Chang, M. Lu, Corrosion of alloy steels containing 2% chromium in $CO_2$ environments, Corrosion Sci. 63 (2012) 246.
[38] Y. Xie, L. Xu, C. Gao, W. Chang, M. Lu, Corrosion behavior of novel 3%Cr pipeline steel in $CO_2$ top-of-line corrosion environment, Mater. Des. 36 (2012) 54.
[39] R.M. Moreira, C.V. Franco, C.J.B.M. Joia, S. Giordana, O.R. Mattos, The effects of temperature and hydrodynamics on the $CO_2$ corrosion of 13Cr and 13Cr5Ni2Mo stainless steels in the presence of free acetic acid, Corrosion Sci.

46 (2004) 2987.
[40] T. Li, Y. Yang, K. Gao, M. Lu, Mechanism of protective film formation during $CO_2$ corrosion of X65 pipeline steel, J. Univ. Sci. Technol. Beijing Miner. Metall. Mater. 15 (2008) 702.
[41] S.D. Zhu, G.S. Zhou, J. Miao, R. Cai, J.F. Wei, Mechanical properties of $CO_2$ corrosion scale formed at different temperatures and their relationship to corrosion rate, Corrosion Eng. Sci. Technol. 47 (2012) 171.
[42] J.K. Heuer, J.F. Stubbins, An XPS characterization of $FeCO_3$ films from $CO_2$ corrosion, Corrosion Sci. 41 (1999) 1231.
[43] A.M. Zimer, E.C. Rios, P.D.C.D. Mendes, W.N. Gonçalves, O.M. Bruno, E.C. Pereira, L.H. Mascaro, Investigation of AISI 1040 steel corrosion in $H_2S$ solution containing chloride ions by digital image processing coupled with electrochemical techniques, Corrosion Sci. 53 (2011) 3193.
[44] O. Sotelo-Mazon, J. Porcayo-Calderon, C. Cuevas-Arteaga, G. Salinas-Solano1, J.J. Ramos-Hernandez, E. Vazquez-Velez, L. Martinez-Gomez, Corrosion performance of Ni-based alloys in sodium metavanadate, Int. J. Electrochem. Sci. 11 (2016) 1868.
[45] C. Yu, X. Gao, H. Wang, Corrosion characteristics of low alloy steel under $H_2S$/$CO_2$ environment: experimental analysis and theoretical research, Mater. Lett. 15 (2017) 459.
[46] Z. Liu, X. Gao, L. Du, J. Li, P. Li, C. Yu, R.D.K. Misra, Y. Wang, Comparison of corrosion behaviour of low-alloy pipeline steel exposed to $H_2S$/$CO_2$-saturated brine and vapour-saturated $H_2S$/$CO_2$ environments, Electrochem. Acta 232 (2017) 528.
[47] Z. Liu, X. Gao, J. Li, L. Du, C. Yu, P. Li, X. Baia, Corrosion behaviour of low-alloy martensite steel exposed to vapour-saturated $CO_2$ and $CO_2$-saturated brine conditions, Electrochem. Acta 213 (2016) 842.
[48] I.B. Singh, M. Singh, S. Das, A comparative corrosion behavior of Mg, AZ31 and AZ91 alloys in 3.5% NaCl solution, J. Magn. Alloys 3 (2015) 142.
[49] Y. Xiao, J. Gu, J. Zhang, Semiconductor property and corrosion behavior of passive film formed on steel with zinc coating in 5% NaCl solution, Arab. J. Sci. Eng. 42 (2017) 4273.
[50] F. Zhu, Y.F. Yin, R.G. Faulkner, Microstructural control of maraging steel C300, Mater. Sci. Technol. 27 (2011) 395.
[51] D.A. López, W.H. Schreiner, S.R. de Sánchez, S.N. Simison, The influence of carbon steel microstructure on corrosion layers an XPS and SEM characterization, Appl. Surf. Sci. 207 (2003) 69.
[52] D.A. López, T. Pérez, S.N. Simison, The influence of microstructure and chemical composition of carbon and low alloys steels in $CO_2$ corrosion. A state-of-the-art appraisal, Mater. Des. 24 (2003) 561.
[53] P. Kumar, M. Singh, R.K. Sharma, G.B. Reddy, An experimental study: role of different ambient on sulfurization of $MoO_3$ into $MoS_2$, J. Alloys Compd. 671 (2016) 440.
[54] M. El-Shamy, F.M. Alkharafi, R.M. Abdallah, I.M. Ghayad, Electrochemical oxidation of hydrogen sulfide in polluted brines using porous graphite electrodes under geothermal conditions, Chem. Sci. J. 1 (2010) 1.
[55] B.G. Ateya, F.M. Al Kharafi, A.M. El-Shamy, A.Y. Saad, R.M. Abdalla, Electrochemical desulfurization of geothermal fluids under high temperature and pressure, J. Appl. Electrochem. 39 (2009) 383.
[56] S.C. Han, H.S. Kim, M.S. Song, P.S. Lee, J.Y. Lee, H.J. Ahn, Electrochemical properties of NiS as cathode material for rechargeable lithium batteries prepared by mechanical alloying, J. Alloys Compd. 349 (2003) 290.
[57] J. Duan, B. Hou, Z. Yu, Characteristics of sulfide corrosion products on 316L stainless steel surfaces in the presence of sulfate-reducing bacteria, Mat. Sci. Eng. 26 (2006) 624.
[58] J. E Thomas, W.M. Skinner, R. St, C. Smart, Comparison of the dissolution behavior of troilite with other iron(II) sulfides; implications of structure, Geochim. Cosmochim. Acta 67 (2003) 831.
[59] J.E. Thomas, C.F. Jones, W.M. Skinner, R.S.t.C. Smart, The role of surface sulfur species in the inhibition of pyrrhotite dissolution in acid conditions, Geochim. Cosmochim. Acta **62** (1998) 1555.
[60] W.Y. Lai, W.Z. Zhao, Z.F. Yin, J. Zhang, EIS and XPS studies on passive film of AISI 304 stainless steel in diluted sulfuric acid solution, Surf. Interface Anal. 44 (2012) 418.
[61] A.P. Grosvenov, B.A. Kobe, M.C. Biesinger, N.S. McIntyre, Investigation of multiplet splitting of Fe2p XPS spectra and bonding in iron compounds, Surf. Interface Anal. 36 (2004) 1564.
[62] P.F. Luo, D.K. Paul, P.M.A. Sherwood, Electrochemical and XPS study of the nickel-titanium electrode, Surf. Anal. Chem. 68 (1996) 3330.
[63] L.J. Liu, Y. Chen, Z.F. Zhang, X.L. You, M.D. Walle, Y.J. Li, Y.N. Liu, Electrochemical reaction of sulfur cathodes with Ni foam current collector in Li-S batteries, J. Power Source 325 (2016) 301.
[64] H.W. Nesbitt, D. Legrand, G.M. Bancroft, Interpretation of Ni2p XPS spectra of Ni conductors and Ni insulators, Phys. Chem. Miner. 27 (2000) 357.
[65] S. Surendran, K.V. Sankar, L.J. Berchmans, R.K. Selvan, Polyol synthesis of α-NiS particles and its physico-chemical properties, Mater. Sci. Semicond. Process. 33 (2015) 16.
[66] X. Shang, X. Lia, W.H. Hua, B. Dong, Y.R. Liu, G.Q. Han, Y.M. Chai, Y.Q. Liu, C.G. Liu, In situ growth of $Ni_xS_y$ controlled by surface treatment of nickel foam as efficient electrocatalyst for oxygen evolution reaction, Appl. Surf. Sci. 378 (2016) 15.
[67] D. Dinda, Md. Estak, S. Mandal, B. Mondai, S.K. Saka, Amorphous molybdenum sulfide quantum dots: an efficient hydrogen evolution catalyst in neutral medium, ACS Catal. 2 (2012) 1916.
[68] Y.R. Liu, J.X. Gou, X. Li, B. Dong, G.Q. Han, W.H. Hu, X. Shang, Y.M. Chai, Y.Q. Liu, C.G. Liu, Self-sacrificial template method of $Mo_3O_{10}(C_6H_8N)_2.2H_2O$ to fabricate $MoS_2$/carbon-doped $MoO_2$ nanobelts as efficient electrocatalyst for hydrogen evolution reaction, Electrochim. Acta 216 (2016) 397.
[69] P. Kumar, M. Singh, R.K. Sharma, G.B. Reddy, An experimental study: role of different ambient on sulfurization of $MoO_3$ into $MoS_2$, J. Alloys Compd. 671 (2016) 440.
[70] O. Mari-Flores, L. Scudiero, S. Há, X-ray diffraction and photoelectron spectroscopy studies of $MoO_2$ as catalyst for the partial oxidation of isooctane, Surf. Sci. 603 (2009) 2337.